Supporting Information for "Energetic Costs of Calcification Under Ocean Acidification"

Christopher Spalding[1], Seth Finnegan[2] and Woodward W. Fischer[1]

Introduction

In the main text, we computed the energetic costs associated with calcification in a batch-like framework and compared these costs to experimentally-derived estimates of organic matrix costs. Section 1 provides a more detailed derivation of the solutions to equations provided in the main text. We also provide extra calculations to analyse the model's sensitivity to various assumptions, including the cost of the organic matrix. In Section 2, we provide an analysis of a steady state model describing calcification, as

[1]Division of Geological and Planetary Sciences, California Institute of Technology, 1200 E. California Blvd., Pasadena, CA, 91125, USA.

[2]Department of Integrative Biology, University of California, 1005 Valley Life Sciences, Bldg #3140, Berkeley, CA, 94720, USA.

opposed to the "batch" model discussed in the main text. This is to illustrate the subtle similarities and differences, and how they might affect the results. Finally, in Section 3 we discuss evidence for the tight kinetic constraints imposed upon larval development that are mentioned in the main text.

1. Solutions to the Calcification Model Equations

Within the main text, we presented the following set of equations describing the time evolution of Total Alkalinity ([TA]) and Dissolved Inorganic Carbon ([DIC])

$$\begin{aligned} V\frac{d[\mathrm{TA}]}{dt} &= 2R_{\mathrm{p}} \\ V\frac{d[\mathrm{DIC}]}{dt} &= \tilde{v}\,A\,\Delta[\mathrm{CO}_2], \end{aligned} \tag{1}$$

Qualitatively, these equations describe a closed-off parcel of water where the left hand side denotes the changing total number of moles of Total Alkalinity and DIC. The right hand side reflects the fact that alkalinity is only added through the removal of hydrogen ions whereas DIC is only changing due to a diffusive flux of CO_2. This form assumes that there is no precipitation of $CaCO_3$ (a sink for both alkalinity and DIC) until we reach the end-point (discussed below). This latter assumption is in part for ease of calculation, but is motivated by the widespread presence of ACC as a precursor in calcifying organisms, which is highly unstable and so forms rapidly when the fluid becomes sufficiently alkaline.

In addition, we approximate the carbonate ion concentration as (*Zeebe & Wolf-Gladrow,* 2001):

$$[\mathrm{CO}_3^{2-}] \approx [\mathrm{TA}] - [\mathrm{DIC}]. \tag{2}$$

In order to remove some of the unknown quantities within these equations, we non-dimensionalized the variables using the following scaling relations:

$$\mathcal{F} = \tilde{v}\, A\, \Delta[\mathrm{CO_2}]$$

$$R_\mathrm{p} = \epsilon\, \mathcal{F}$$

$$\mathcal{T} = \frac{V[\mathrm{DIC}]_\mathrm{sw}}{\mathcal{F}}. \tag{3}$$

Denoting the dimensionless variables by the use of a prime (e.g. $[\mathrm{TA}] = [\mathrm{TA}]'[\mathrm{DIC}]_\mathrm{sw}$, $t = t'\mathcal{T}$, etc) we substitute the above relations into Eqs. (1) to obtain the dimensionless ordinary differential equations:

$$\frac{d[\mathrm{TA}]'}{dt'} = 2\epsilon$$
$$\frac{d[\mathrm{DIC}]'}{dt'} = 1, \tag{4}$$

and therefore, using equation (2),

$$\frac{\mathrm{d}[\mathrm{CO_3^{2-}}]'}{\mathrm{d}t'} = 2\epsilon - 1. \tag{5}$$

These differential equations are straight-forward to solve. We integrate with respect to dimensionless time t' and use seawater as the initial condition. As in the main text, we parameterize this initial condition by way of x_2, the bicarbonate fraction of DIC in seawater. If we ignore the contribution to seawater DIC from dissolved $\mathrm{CO_2}$, the initial $[\mathrm{CO_3^{2-}}]'|_{t'=0} = 1 - x_2$. We present the solutions for [DIC] and carbonate ion

$$[\mathrm{CO_3^{2-}}]' = (2\epsilon - 1)t' + (1 - x_2)$$

$$[\mathrm{DIC}]' = 1 + t'. \tag{6}$$

As discussed in the main text, in order to compute a cost, we must decide when the pumping process reaches a given end-point ($t' = t'_\mathrm{end}$). This end-point is prescribed by

supposing that the final concentration of carbonate is some fraction γ of the total DIC in the calcifying fluid. We chose $\gamma = 0.5$, which corresponds to pH=pK$_2$, but here we will derive the cost for general γ in order to illustrate the dependence of our solution upon γ.

From equation (6), the relevant equation to solve is

$$[\mathrm{CO}_3^{2-}]'\big|_{t'_{\mathrm{end}}} = \gamma[\mathrm{DIC}]\big|_{t'_{\mathrm{end}}}$$

$$(2\epsilon - 1)t'_{\mathrm{end}} + (1 - x_2) = \gamma\,(1 + t'_{\mathrm{end}}) \tag{7}$$

yielding the end-time

$$t'_{\mathrm{end}} = \frac{1 - x_2 - \gamma}{1 + \gamma - 2\epsilon}. \tag{8}$$

1.1. Calculating Cost and Susceptibility.

Having obtained an end time to the pumping, we can now compute the amount of energy expended by the organism per gram of $\mathrm{CaCO_3}$ precipitated. The number of Calcium ions pumped in time t is given by $R_{\mathrm{p}}\,t$, which can be multiplied by the molar cost of ATP ($\eta = 30\,\mathrm{kJ\,mol^{-1}}$) to obtain the metabolic cost at time t. At the end-point, the number of moles of $\mathrm{CaCO_3}$ obtained from the process is given by $[\mathrm{DIC}]_{\mathrm{sw}}\,V\,\gamma(1 + t'_{\mathrm{end}})$. Finally, we use the molar mass of $\mathrm{CaCO_3}$ ($\mu_{\mathrm{C}} = 100\,\mathrm{g\,mol^{-1}}$) to convert moles to grams, yielding a cost per gram of

$$\begin{aligned}
\mathcal{C} &\equiv \frac{\text{energy expended}}{\text{mass of } \mathrm{CaCO_3}} \\
&= \frac{\eta R_{\mathrm{p}} t'_{\mathrm{end}} \mathcal{T}}{\mu_{\mathrm{C}} V [\mathrm{DIC}]_{\mathrm{sw}} [\mathrm{CO}_3^{2-}]'|_{t'_{\mathrm{end}}}} \\
&= \frac{\eta}{\mu_{\mathrm{C}}} \frac{\epsilon t'_{\mathrm{end}}}{\gamma(1 + t'_{\mathrm{end}})} \\
&= \frac{\eta}{\mu_{\mathrm{C}}} \frac{x_2 - 1 + \gamma}{\gamma\,(x_2 - 2(1 - \epsilon))}\,\epsilon,
\end{aligned} \tag{9}$$

where the substitution $\gamma = 1/2$ yields equation (9) of the main text.

Note that in the above equation, if the organism is pumping relatively fast such that $\epsilon - 1 \gg x_2/2$, the cost per gram increases linearly with x_2, the bicarbonate fraction of the original seawater.

1.2. Metabolic Carbon

The parameter ϵ is difficult to measure, however the metabolic carbon fraction f_{M} of bivalve shells has been measured and tracked throughout ontogeny (*Waldbusser et al.,* 2013). Therefore, we choose to present our results in terms of the measurable f_{M}.

The amount of metabolic carbon within the calcifying fluid in our model at time t' is simply the difference between the initial DIC and the DIC at time t' (because the only DIC added is metabolic). The initial DIC in dimensionless units is unity and its time evolution is given by Equation (6). Therefore, the amount of metabolic carbon in dimensionless units is simply equal to t'. Accordingly, the metabolic fraction (f_{M}) as a function of time is:

$$\begin{aligned} f_{\mathrm{M}} &= \frac{\text{metabolic DIC}}{\text{total DIC}} \\ &= \frac{t'}{1+t'}. \end{aligned} \tag{10}$$

If we now substitute $t' = t'_{\mathrm{end}}$, we obtain the expected metabolic carbon fraction present in the final, inorganic portion of the shell precipitated by the organism,

$$f_M|_{t'_{\mathrm{end}}} = \frac{x_2 - 1 + \gamma}{2\left(\epsilon - 1\right) + x_2}, \tag{11}$$

which leads to equation (13) of the main text upon setting $\gamma = 1/2$. As discussed in the main text, the rate of calcification $\mathcal{R}$ is simply related to f_{M} through

$$\mathcal{R} = \frac{\gamma}{f_{\mathrm{M}}}. \tag{12}$$

We can rearrange our relation between $f_{\rm M}$ and ϵ within the batch model,

$$\epsilon = \frac{f_{\rm M}(2 - x_2) + x_2 - 1 + \gamma}{2 f_{\rm M}}, \tag{13}$$

to explicitly write the batch cost in terms of $f_{\rm M}$:

$$\mathcal{C} = \frac{\eta}{\mu_{\rm C}} \frac{f_{\rm M}(2 - x_2) + x_2 + \gamma - 1}{2\gamma} \tag{14}$$

1.3. Whole Skeleton Costs

As discussed in the main text, the energetic cost of the entire skeleton includes components arising from organic parts embedded within the shell. This organic material will have associated with it a cost per mass ν. Accordingly, if a mass fraction $f_{\rm p}$ of the shell is organic, the total energetic cost $\mathcal{E}$ per mass of skeleton becomes

$$\begin{aligned} \mathcal{E}(x_2, f_{\rm p}) &\equiv \frac{\text{inorganic cost} + \text{organic cost}}{\text{total mass}} \\ &= \frac{\mathcal{C} \times (\text{inorganic mass}) + \nu \times (\text{organic mass})}{\text{total mass}} \\ &= \mathcal{C}(1 - f_{\rm p}) + \nu\, f_{\rm p}, \end{aligned} \tag{15}$$

where the left term arises from the inorganic costs (derived above) and the right from organic costs.

In the main text, we defined the sensitivity function

$$\mathcal{S} \equiv \frac{1}{\mathcal{E}} \frac{\partial \mathcal{E}}{\partial x_2} \Delta x_2, \tag{16}$$

allowing us to quantify fractional increases in cost. This expression may be thought of conceptually as the fraction increase in the cost per mass ($\Delta\mathcal{E}/\mathcal{E}$) arising as a result of a given, fractional rise in bicarbonate concentration ($\Delta x_2/x_2$). Using the expressions for $\mathcal{C}$

and $\mathcal{S}$, the sensitivity function takes the rather unwieldy form

$$\mathcal{S} = \frac{(1-f_{\rm p})(1+\gamma-2\epsilon)(\eta/\mu_{\rm C})\epsilon\Delta x_2}{(2(\epsilon-1)+x_2)\big[(1-f_{\rm p})(x_2+1-\gamma)(\eta/\mu_{\rm C})-f_{\rm p}\gamma(x_2-2(\epsilon-1)\nu)\big]}. \quad (17)$$

It is this function that we plot (again in terms of $f_{\rm M}$) in the right panels of Figures (S2) and (2) with $\gamma = 0.5$.

Within the main text, we adopted a cost of organic material, $\nu = 30\,{\rm J\,mg^{-1}}$, from the experimental work of *Palmer* (1992). However, the cost of inorganic components remains somewhat uncertain and most likely varies between organisms. Consequently here we present the equivalent results displayed in Figure (2) of the main text, but use instead $\nu = 3\,{\rm J\,mg^{-1}}$, which is a typical cost for simple amino acid synthesis [*Pace and Manahan* 2006, *Pan et al.* 2015].

As can be seen from Figure S2, cheaper organic costs dampen the organic carbon buffering effect upon sensitivity, as is seen by the increase in minimum sensitivity from ∼1.7% to ∼9% between the two cases. On the other hand, the maximum shell costs drop from $\sim 1.6\,{\rm J\,mg^{-1}}$ to $\sim 0.4\,{\rm J\,mg^{-1}}$. However, qualitatively the conclusions remain the same, i.e., that an increased organic component makes for a less sensitive but more expensive shell.

2. Steady-State Model

In the main text, we described a "batch" model, whereby calcification occurs within individual parcels of fluid. Each parcel has its chemistry altered to a given end-point before the $CaCO_3$ precipitates. Such a model is highly idealized and might be better suited to certain calcifying taxa than others. Indeed, some earlier work has considered a

more steady-state calcification scenario as appropriate, particularly to corals (e.g. [*Adkins et al. (2003)*]). In this section we describe a similar model here and compare key features of it to the "batch" model off of which we based our main conclusions.

Consider a compartment of fluid that is maintained at a constant chemical composition whilst undergoing continuous exchange with seawater. For a steady state to exist, all fluxes of DIC and Alkalinity must balance: The DIC lost through $CaCO_3$ precipitation must be replaced through a combination of seawater mixing and metabolic carbon influx. Likewise, all alkalinity removed through precipitation must be replenished by the Ca-ATPase pumps, together with mixing of alkalinity from seawater. From the outset we note that the steady-state model may be conceptualized as an average over many batches. The instantaneous calcification rate in the former scenario is constant, whereas in the latter scenario the rate is impulsive, with precipitation occurring each time a parcel reaches the end-point. However, in terms of the mass-specific cost of an entire skeleton, both viewpoints are equivalent.

As with the batch process described in the main text, we can model the steady state process using a system of equations, scaled by the same dimensional quantities ($\mathcal{F}$, $\mathcal{T}$, $[\mathrm{DIC}]_{\mathrm{sw}}$). However, here we must include a term that reflects the mixing with seawater, parameterized as a timescale $\tau = |\tau'|\mathcal{T}$ over which the calcifying fluid is replaced by seawater, where $||$ denotes absolute value. The steady state equations are simple to write down:

$$\begin{aligned} \epsilon_c - \epsilon_p &= \frac{1}{2|\tau'|}([\mathrm{TA}]'_{\mathrm{sw}} - A') \\ \epsilon_c - 1 &= \frac{1}{|\tau'|}([\mathrm{DIC}]'_{\mathrm{sw}} - C') \end{aligned} \tag{18}$$

where we have defined the dimensionless pumping rate ϵ_p (equivalent to the parameter ϵ used in the batch model) and the dimensionless calcification rate ϵ_c. Both theses rates are again scaled relative to the influx of metabolic CO_2. In addition, A' and C' are, respectively, the Total Alkalinity and DIC of the calcifying fluid, scaled by the concentration of DIC in seawater. Note that the analogous quantities in the batch model above were labelled $[\mathrm{TA}]'$ and $[\mathrm{DIC}]'$, but we chose different variables (as we did with ϵ_p) in order to clearly distinguish the two models.

The quantities $[\mathrm{TA}]'_\mathrm{sw}$ and $[\mathrm{DIC}]'_\mathrm{sw}$ are the analogously-scaled properties of seawater, such that

$$[\mathrm{TA}]'_\mathrm{sw} \approx x_2 + 2x_3 \approx 2 - x_2$$

$$[\mathrm{DIC}]'_\mathrm{sw} \approx x_2 + x_3 \approx 1, \tag{19}$$

where x_3 is defined as the carbonate fraction of seawater DIC, as opposed to x_2, the bicarbonate fraction. The right hand sides of Equations (18) arise from mixing with seawater. The situation where $|\tau'| \to \infty$ represents a perfectly sealed parcel of seawater, i.e. the batch model, when a steady state only exists if $\epsilon_\mathrm{c} = \epsilon_\mathrm{p} = 1$.

It is worth pointing out two immediate properties and limitations of the steady state scenario. First, in order to maintain a concentration of DIC in the fluid greater than that of seawater (as suggested by some studies on corals; *Allison et al.* [2014]), the only source of DIC capable of balancing calcification and seawater mixing is diffusion of metabolic CO_2 into the space. Such a diffusion-limited strategy might be favoured by organisms that host symbiotic photosynthesizers and potentially helps decouple their calcification from seawater conditions.

Second, as with the batch process, we can write down an expression for the metabolic carbon fraction f_{M} of the calcifying fluid. Specifically, keeping track only of the metabolic carbon, we can write the steady state equation

$$\epsilon_c f_{\mathrm{M}} - 1 = -\frac{f_{\mathrm{M}} C'}{\tau'}, \tag{20}$$

which can be rearranged, using equation 18 to obtain

$$f_{\mathrm{M}} = \frac{|\tau'|}{1 + |\tau'|}. \tag{21}$$

Recall from the main text that the batch model led to a metabolic fraction

$$f_{\mathrm{M}}\big|_{\mathrm{batch}} = \frac{t'_{\mathrm{end}}}{1 + t'_{\mathrm{end}}}, \tag{22}$$

which takes a very similar functional form to the steady state scenario. This similarity is not a coincidence; the end time t'_{end} of the batch process is the timescale over which an old parcel of seawater has had its chemistry altered to the required degree and a new parcel of seawater must be obtained. Likewise, τ' is the timescale over which the entire calcifying space is replaced by new seawater, which is equivalent to averaging over many parcels in the batch process.

Relation 21 allows us to replace the seawater exchange timescale $|\tau'|$ with an observable quantity, f_{M} in the steady state equations above:

$$\begin{aligned} \epsilon_c - \epsilon_p &= \frac{1}{2}\left(\frac{1 - f_{\mathrm{M}}}{f_{\mathrm{M}}}\right)([\mathrm{TA}]'_{\mathrm{sw}} - A') \\ \epsilon_c - 1 &= \left(\frac{1 - f_{\mathrm{M}}}{f_{\mathrm{M}}}\right)([\mathrm{DIC}]'_{\mathrm{sw}} - C'). \end{aligned} \tag{23}$$

As we did before, we now assume that the fluid is maintained at $p\mathrm{K}_2$ ($[\mathrm{CO}_3^{2-}] = [\mathrm{HCO}_3^-] = [\mathrm{DIC}]/2$). This removes one degree of freedom by allowing us to write

$$\begin{aligned} A' &= (2[\mathrm{CO}_3^{2-}] + [\mathrm{HCO}_3^-])/[\mathrm{DIC}]_{\mathrm{sw}}. \\ &= \frac{3}{2}C', \end{aligned} \tag{24}$$

Accordingly, we may again rewrite the steady state equations as

$$\begin{aligned} \epsilon_c - \epsilon_p &= \frac{1}{2}\left(\frac{1-f_{\mathrm{M}}}{f_{\mathrm{M}}}\right)([\mathrm{TA}]'_{\mathrm{sw}} - 3C'/2) \\ \epsilon_c - 1 &= \left(\frac{1-f_{\mathrm{M}}}{f_{\mathrm{M}}}\right)([\mathrm{DIC}]'_{\mathrm{sw}} - C'), \end{aligned} \tag{25}$$

which we can now solve.

2.1. Cost comparison

The steady state cost $\mathcal{C}_{\mathrm{ss}}$ is computed in an analogous fashion to the batch process — the energy expended per gram of calcium carbonate precipitated:

$$\mathcal{C}_{\mathrm{ss}} \equiv \frac{\eta}{\mu_C}\frac{\epsilon_p}{\epsilon_c}. \tag{26}$$

Through algebraic manipulation of the simultaneous equations (25), we solve for both ϵ_{c} and ϵ_{p} in terms of the observables f_{M} and C'. Substituting into the expression above for cost yields the result:

$$\begin{aligned} \mathcal{C}_{\mathrm{ss}} &= \frac{\eta}{\mu_{\mathrm{C}}}\frac{C' - 4|\tau'| - 2x_2}{4(1 - C' + |\tau'|)} \\ &= \frac{\eta}{\mu_{\mathrm{C}}}\frac{f_{\mathrm{M}}(2-x_2) + x_2 + C'(f_{\mathrm{M}}-1)/2}{2(1 + C'(f_{\mathrm{M}}-1))}. \end{aligned} \tag{27}$$

The final step is to compare this cost to the cost derived in the batch model,

$$\mathcal{C} = \frac{\eta}{\mu_{\mathrm{C}}}\frac{f_{\mathrm{M}}(2-x_2) + x_2 + \gamma - 1}{2\gamma}. \tag{28}$$

The expressions are identical in the limiting case where $C' = 0$ and $\gamma = 1$. This is not entirely surprising because $\gamma = 1$ means that all of the DIC taken up in each parcel is precipitated as $CaCO_3$ whereas $C' = 0$ analogously means that precipitation draws all the DIC in the calcifying space out into $CaCO_3$ much faster than new seawater is brought in. In other words, the steady state calcifying space acts as one big "parcel".

In order to compare the costs we define a ratio of the batch cost to the steady state cost as

$$\begin{aligned} r_{\mathrm{C}} &\equiv \frac{\mathcal{C}}{\mathcal{C}_{\mathrm{ss}}} \\ &= \left(\frac{f_{\mathrm{M}}(2 - x_2) + x_2 + \gamma - 1}{2\gamma} \right) \\ &\times \left(\frac{2(1 + C'(f_{\mathrm{M}} - 1))}{f_{\mathrm{M}}(2 - x_2) + x_2 + C'(f_{\mathrm{M}} - 1)/2} \right) \end{aligned} \tag{29}$$

In Figure 3, we plot this ratio as a function of C' for 4 different choices of f_{M} (0, 0.1, 0.3, 0.5) spanning the range measured in bivalve shells (*Gillikan et al.,* 2007; *Waldbusser et al.,* 2013), along with $\gamma = 1/2$. As can be seen, the costs are rather similar across a wide range of C', however, there exist C' for which the steady state cost is much greater than the batch cost. In principle, C' is measurable, but such measurements are limited and different experimental assumptions can cause the inferred C' to vary from much less than unity to greater than unity (for example, assumptions upon borate precipitation *Allison et al.*, 2014).

Given the uncertainty in C', we work with the assumption that organisms will function such as to minimize costs for their given physiology. Therefore, we neglect the cases where C' is kept at the value where costs become very large (Figure 3), in which case the batch and steady state models yield similar costs. However, we maintain the caveat that in

some special cases the inorganic costs may in fact be higher than those derived in the main text.

3. Larval Growth Curves

In the main text, we discussed how larvae are subject to kinetic calcification constraints not felt as intensely during their adult stages. This notion is supported by observations from a wide range of taxa in which the growth rates relative to body size of larval forms are vastly in excess of those typical of adults of the same species. In Figure (S4), we illustrate growth curves obtained experimentally for the brachiopod *Terebratalia transversa* (data from *Stricker and Reed*, (1985)) and the oyster *Crassostrea gigas* (data from *Waldbusser et al.*, 2013) for the first weeks of the species' development, which display a significant nonlinear drop in calcification rate after the first couple of days of life during which the skeleton is first synthesized.

References

Allison, N., Cohen, I., Finch, A. A., Erez, J., & Tudhope, A. W. (2014). Corals concentrate dissolved inorganic carbon to facilitate calcification. Nature communications, 5.

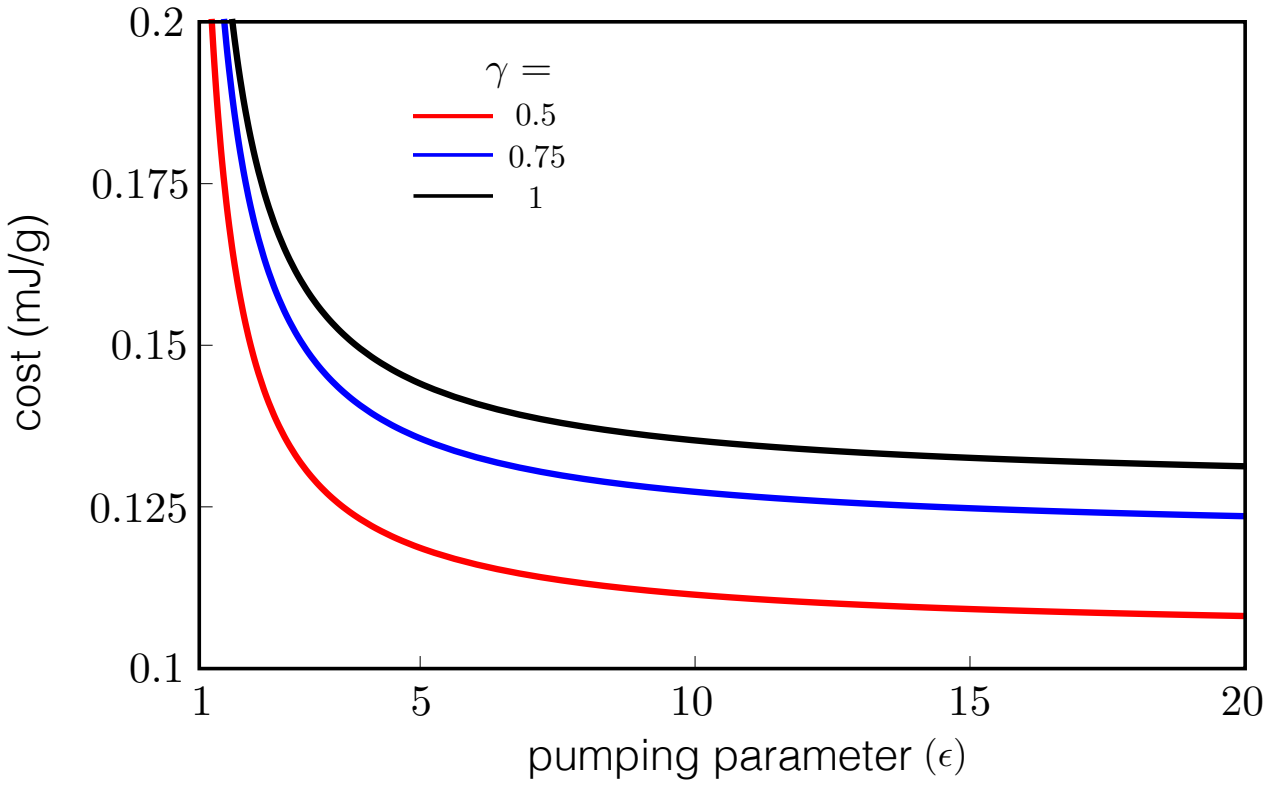

Figure 1. Illustration of the dependence of our computed cost upon our choice of γ. The red (lowest) line corresponds to our chosen value of $\gamma = 0.5$. The blue has $\gamma = 0.75$ and gold $\gamma = 1$. The upper curve is roughly 40% larger than the lowest curve, suggesting that our inferred costs may differ by a comparable degree to reality. However, stopping at pK_2 makes sense on chemical grounds, and agrees with the pH observed in the calcifying fluids of multiple organisms.

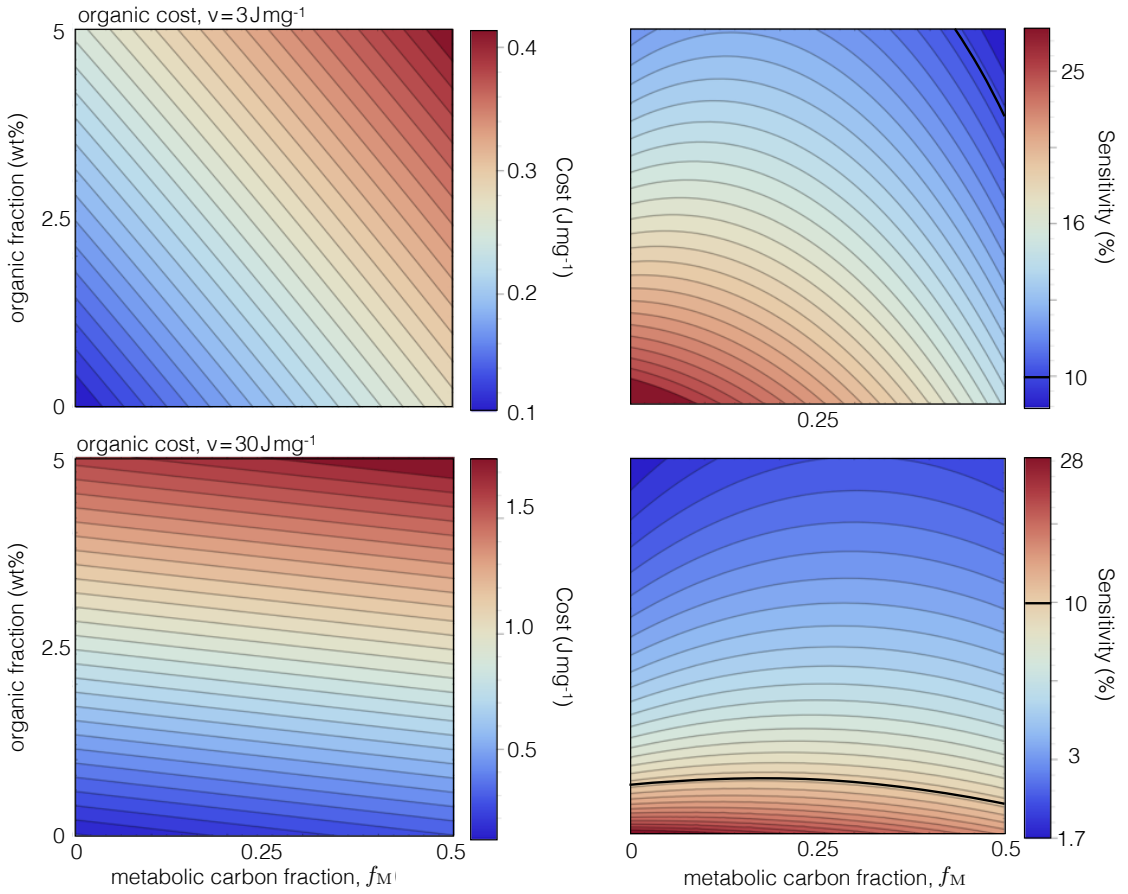

Figure 2. A comparison between the susceptibility and costs obtained using a value of $\nu = 30\,\mathrm{J\,mg^{-1}}$ (upper panels, *Pace and Manahan*, 2006; *Pan et al.*, 2015) and a value 10 times smaller (lower panels, *Pace and Manahan* 2006; *Pan et al.* 2015). The thick grey line indicates a sensitivity of 10%. Notice that the qualitative trend is similar in both cases but the results change quantitatively. Specifically, the ability of additional organic material to decrease susceptibility is less pronounced when the organic material itself (and therefore the skeleton) is cheaper.

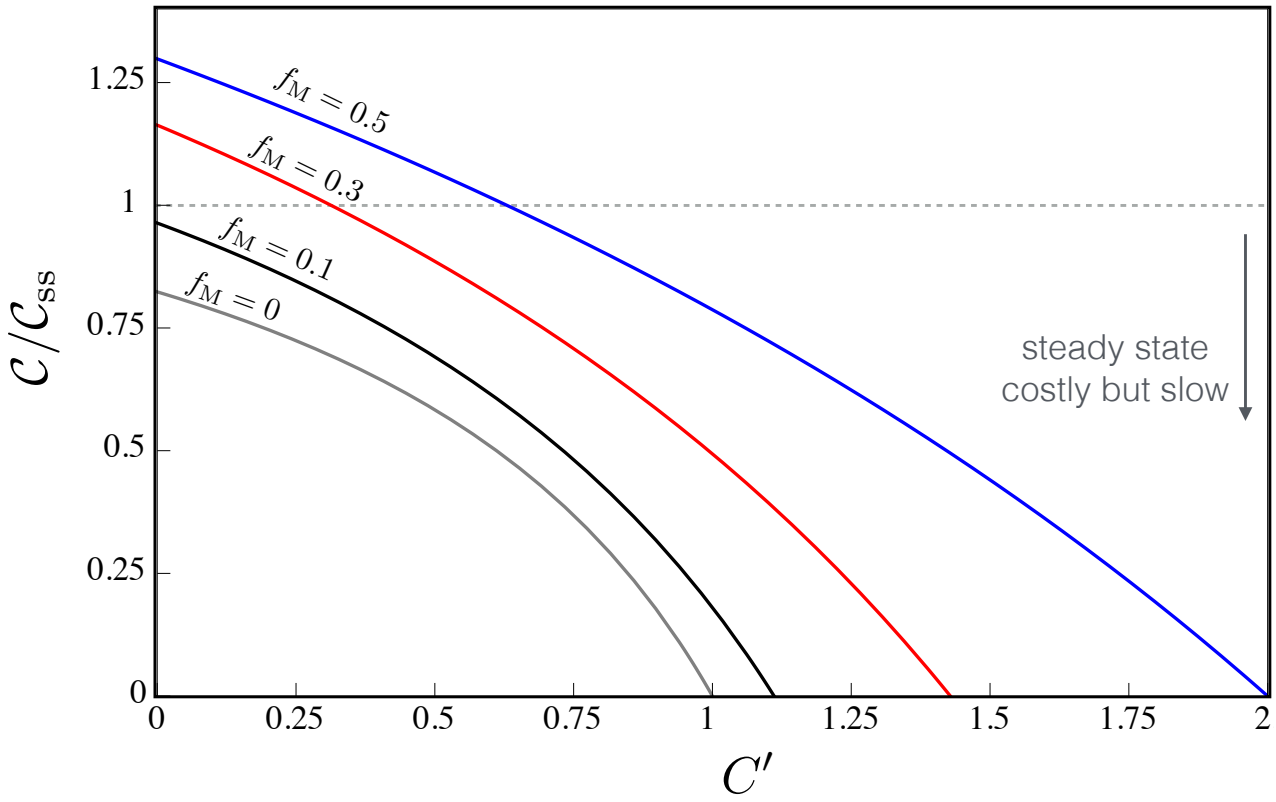

Figure 3. Ratio of inorganic costs between the batch model ($\mathcal{C}$) and the steady state model $\mathcal{C}_{ss}$. The x-axis denotes the scaled DIC concentration in the steady-state calcifying space. We plot the ratio for four metabolic carbon fractions f_M =(0, 0.1, 0.3 and 0.5), which span the observed range in bivalve shells (*Gillikan et al.,* 2007; *Waldbusser et al.,* 2013). The steady state costs are sensitive to the parameter C' and can be either greater or less than those of the batch model, but assuming the organism is aiming to calcify rapidly, we work under the assumption that C' does not lie in the range where $\mathcal{C}_{ss} \gg \mathcal{C}$.

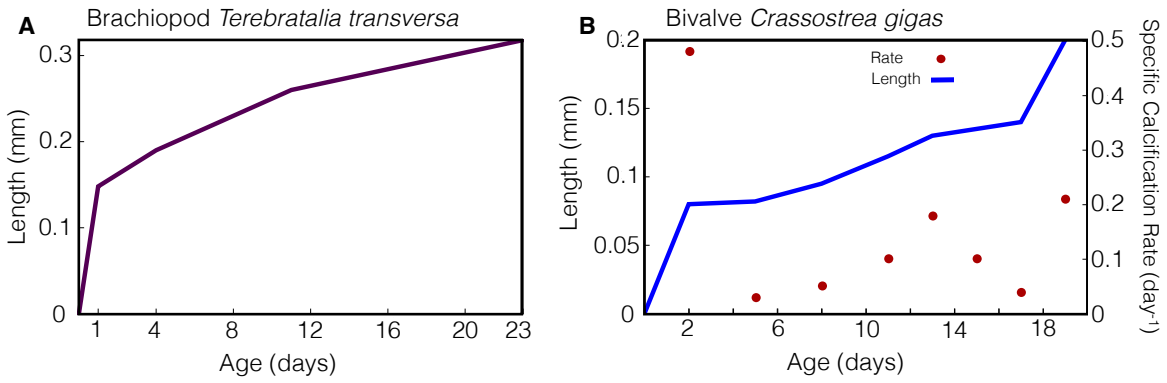

Figure 4. Published growth curves for the first ∼20 days of life for A). the brachiopod *Terebratalia transversa* [*Stricker and Reed* (1985)] and B). the oyster (a bivalve) *Crassostrea gigas* [*Waldbusser et al.* (2013)]. Notice that for both species, the absolute rate of shell growth is vastly greater in the first 1-2 days than during the later stages. Furthermore, as is evident from B., not only is the absolute growth rate (blue line) vastly greater in the earliest stages, but as is the specific growth rate (red circles), the increase in shell mass as a fraction of current shell mass. This figure illustrates the pressure to form the earliest parts of the shell more quickly than subsequent parts.